

CHOSEN ASPECTS OF INVESTIGATIONS OF SOLAR CELLS WITH THE LASER BEAM INDUCED CURRENT TECHNIQUE

Łukasz Bartłomiej Chrobak, Wiesław Ryszard Madej, Mirosław Andrzej Maliński

Koszalin University of Technology, Department of Electronics and Computer Sciences, Śniadeckich 2, 75-453 Koszalin, Poland
(✉ lukasz.chrobak@tu.koszalin.pl, +48 94 343 3485, madej@ie.tu.koszalin.pl, mmalin@tu.koszalin.pl)

Abstract

This paper presents maps of spatial distributions of the short circuit current $I_{sc}(x,y)$ and the open circuit voltage $U_{oc}(x,y)$ of the investigated low cost solar cells. Visible differences in values of these parameters were explained by differences in the serial and shunt resistances determined for different points of solar cells from measurements of I–V characteristics. The spectral dependence of the photo voltage of solar cell is also shown, discussed and interpreted in the model of amorphous and crystal silicon.

Keywords: nondestructive techniques, laser beam induced current, photovoltaics, silicon, solar cells, I–V characteristics, optical absorption coefficient spectra.

© 2015 Polish Academy of Sciences. All rights reserved

1. Introduction

The photovoltaic industry still grows globally what leads a solar cell research to be more important nowadays. The main advantage of the solar power is its environmentally friendly character. Due to its wide availability, silicon is the most important material applied for solar cells manufacturing [1]. Basic types of silicon cells can be listed as: monocrystalline solar cells, polycrystalline solar cells, thin-film crystalline silicon based solar cells and thin-film crystalline amorphous silicon based solar cells [2–4]. For production of widely available solar cells, *i.e.*, garden solar cells, amorphous silicon based cells are used. Production technology of these cells allows for a cost reduction due to the used amorphous material. Moreover, this technology enables also a reduction of the cell thickness. Very often for this type of applications tandem solar cells [5] are used. Typical commercial tandem cells contain two layers. Typical commercial low cost solar cells of this type were investigated with the use of non-destructive laser beam induced current technique (LBIC). Semiconductor materials used for production of solar cells are often not free from many kinds of defects which have a significant impact on their energy efficiency. Most undesirable defects are: diffusion length changes, local serial and shunt resistance changes, surface quality which leads to a decrease of energy efficiency. Characterization and production technology upgrade of solar cells is also possible due to several non-destructive measuring methods, such as: the I–V measurement technique [6, 7], electroluminescence technique [8, 9], infrared imaging technique [10], lock-in thermography technique [11, 12]. In this paper the Laser Beam Induced Current (LBIC) technique has been used [13]. Investigations with the use of laser beams have been performed for the first time in the 70-ies [14, 15]. In the beginning of the use of this technique it was the light source that was a movable element. With time another idea has been proposed which led to a movable solar cell solution [16, 17]. The applications of stepper motors enabled rapid and precise solar cells scanning for detection of undesired defects. In the LBIC technique a fast

laser beam scanning is performed. Due to the photon energy absorption (bigger than a semiconductor energy gap) an electron transition from the valence to conduction band proceeds. This leads to the current induction – its analysis enables extraction of properties of an investigated solar cell, especially its defects. In this paper typical commercial low cost solar cells were investigated with the use of non-destructive laser beam induced current technique, the I-V technique, and a spectral photo voltage technique.

2. Experimental setup and results

The experimental set up which has been built and applied for measurements of the laser beam induced current maps is presented in Fig. 1. It consists of a 50 mW green 532 nm laser with the beam size diameter of 100 μm , a mirror which directs the light beam to the investigated solar cell, X–Y stages for moving the cell, a BNC-2120 module through which the signal is passed to a fast NI USB-6255 measuring card, and a personal computer with a dedicated acquire – control application written in the C++ programming language.

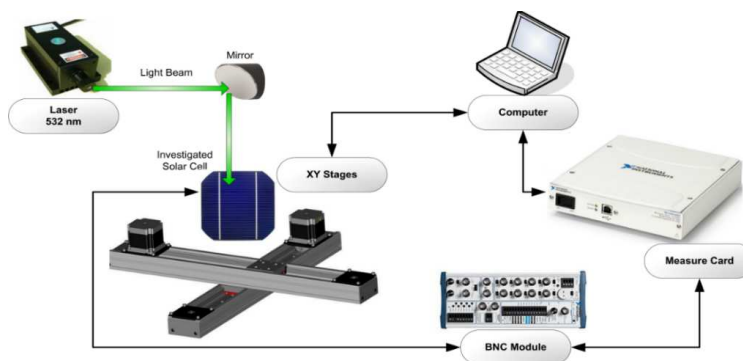


Fig. 1. The experimental set up for laser beam induced current measurements.

All measurements were computer controlled and performed at the room temperature. The spatial distributions of the open circuit voltage $U_{oc}(x,y)$ of investigated solar cell are presented in Figs. 2 and 3.

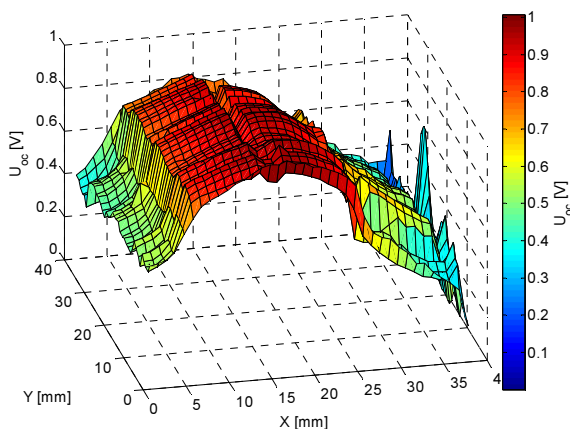


Fig. 2. The surface plot of open circuit LBIC voltage $U_{oc}(x,y)$ values obtained for the investigated solar cell.

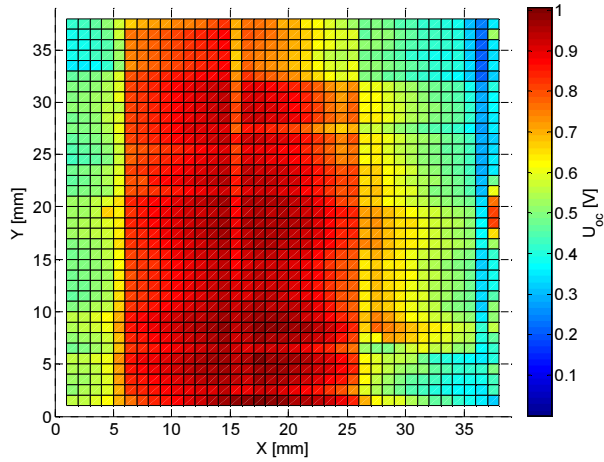


Fig. 3. The map of open circuit LBIC voltage $U_{oc}(x,y)$ values obtained for the investigated solar cell.

The histogram of open circuit voltages $U_{oc}(x,y)$ of the solar cell is presented in Fig. 4.

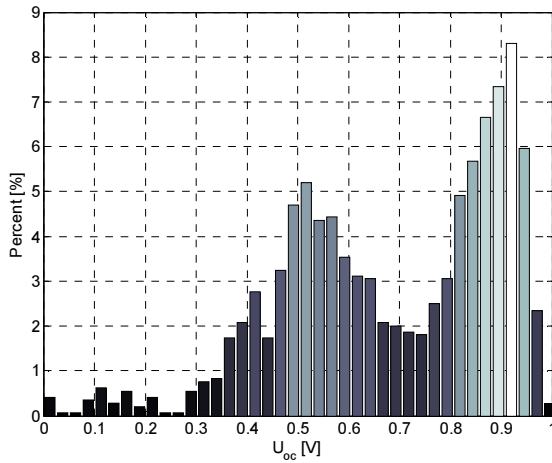


Fig. 4. The histogram of open circuit LBIC voltage $U_{oc}(x,y)$ values obtained for the investigated solar cell.

This histogram shows the percentage part of investigated solar cell surface exhibiting a given value of U_{oc} – from U_{oc} to $U_{oc} + 0.25$ V. For example, this histogram shows that about 50% of the solar cell surface exhibits U_{oc} values within the range from 0.7 V to 0.95 V.

The spatial distributions of the short circuit current $I_{sc}(x,y)$ of investigated solar cell are presented in Figs. 5 and 6.

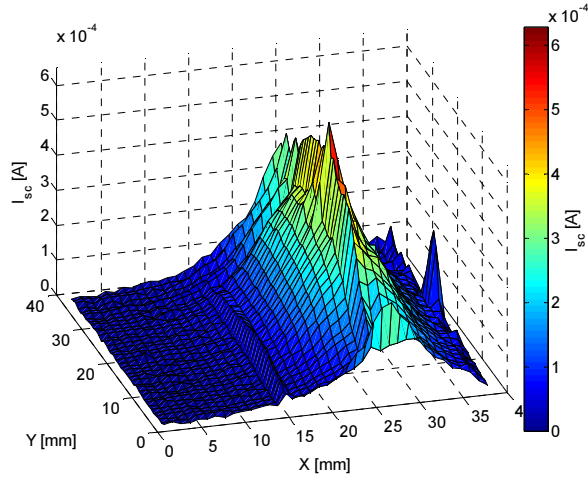


Fig. 5. The surface plot of short circuit LBIC current $I_{sc}(x,y)$ values obtained for the investigated solar cell.

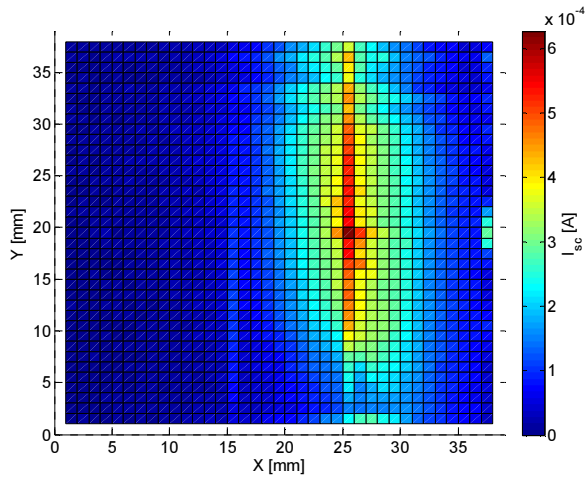


Fig. 6. The map of short circuit LBIC current $I_{sc}(x,y)$ values obtained for the investigated solar cell.

The histogram of short circuit current $I_{sc}(x,y)$ of solar cell is presented in Fig. 7.

This histogram shows the percentage part of investigated solar cell surface exhibiting a given value of I_{sc} – from I_{sc} to $I_{sc} + 0.17 \cdot 10^{-4}$ A. For example, it shows that only 3% of the solar cell surface exhibits I_{sc} values within the range from $4 \cdot 10^{-4}$ A to $6 \cdot 10^{-4}$ A.

To explain the reasons of such huge current differences observed on the LBIC maps the I–V characteristics of solar cell were measured in different points of the map. The single diode model of solar cell used in this paper is presented in Fig. 8.

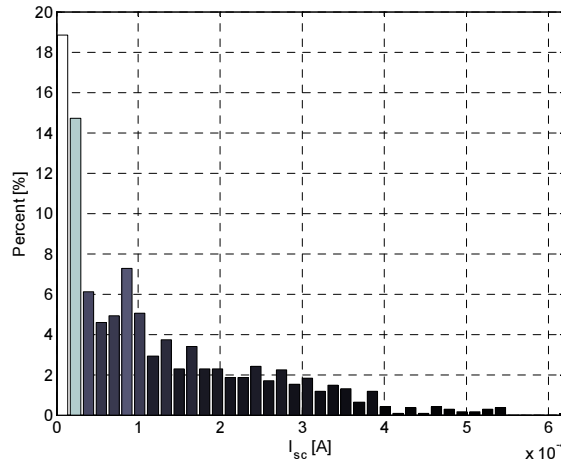


Fig. 7. The histogram of short circuit LBIC current $I_{sc}(x,y)$ values obtained for the investigated solar cell.

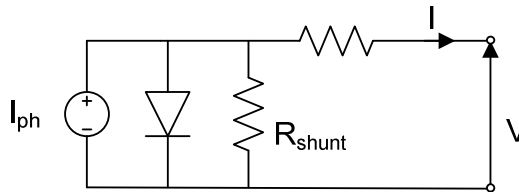


Fig. 8. The electrical circuit equivalent of solar cell (single diode model).

The electrical circuit equivalent of solar cell (relation of the current I and voltage V in the single diode model) can be described by the following (1):

$$I = I_0 \left[\exp \left(\frac{V + I R_{serial}}{n \frac{k_B T}{q}} \right) - 1 \right] + \frac{V + I R_{serial}}{R_{shunt}} - I_{ph}, \quad (1)$$

where I_0 is the reverse saturation current, I_{ph} is the photocurrent, n is the diode ideality factor, k_B is the Boltzmann constant, T is the temperature, q is the elementary charge, R_{serial} is the serial resistance and R_{shunt} is the shunt resistance.

The most important solar cell parameters are: power conversion efficiency (P_{max}), short-circuit current (I_{sc}), open-circuit voltage (V_{oc}) and fill factor (FF). However, in most cases serial and shunt resistance values cannot be neglected and must be extracted – which is not simple. It is known from the literature that the serial and shunt resistances can be found from the slope of output characteristics under dark conditions [19, 20]. This simple method can be used only under assumption that the serial resistance is much smaller than the shunt resistance. There are many other methods which can be used to extract parameters of solar cells from the I–V characteristics [20–28]. The simplest way to obtain essential parameters is to perform fitting the theoretical characteristics (1) to experimental data. The (1) does not have an explicit solution. However, some methods based on the LambertW function have been proposed in papers [25, 26]. The authors of those papers rearranged the (1) to the form presented below:

$$I = -\frac{V}{R_{\text{serial}} + R_{\text{shunt}}} - \frac{n \frac{k_B T}{q}}{R_{\text{serial}}} \text{LambertW}(K) + \frac{R_{\text{shunt}} (I_0 + I_{ph})}{R_{\text{serial}} + R_{\text{shunt}}}, \quad (2)$$

$$K = \frac{R_{\text{serial}} I_0 R_{\text{shunt}} \exp \left[\frac{R_{\text{shunt}} (V + R_{\text{serial}} I_0 + R_{\text{serial}} I_{ph})}{n \frac{k_B T}{q} (R_{\text{serial}} + R_{\text{shunt}})} \right]}{n \frac{k_B T}{q} (R_{\text{serial}} + R_{\text{shunt}})}, \quad (3)$$

where *LambertW* is the LambertW function (also called the omega function) which is defined by the solution of equation $x = W(x)e^{W(x)}$.

In the above presented equations I_{ph} is assumed to be equal to the short circuit current (I_{sc}). The detailed description of this method and (2–3) is presented in papers [25, 26]. This method was used in this work to extract, from the experimental I–V characteristics, essential parameters of investigated solar cells.

The I–V characteristics were measured both at the maximum $I_{sc}(x,y)$ point and at the minimum $I_{sc}(x,y)$ point. These characteristics are presented in Figs. 9 and 10.

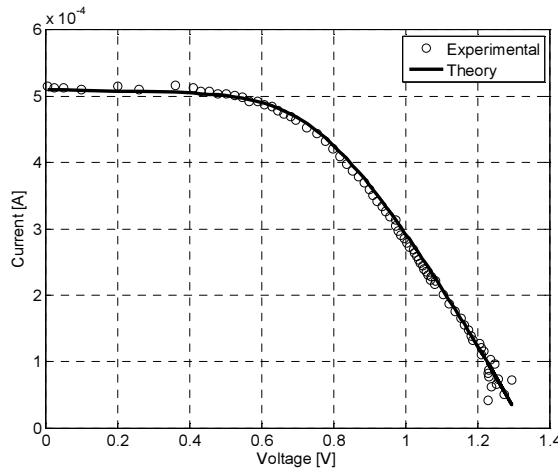


Fig. 9. The experimental data for the investigated silicon cell obtained at the maximum current point (circles) and the I–V theoretical curve calculated for parameter values obtained from the optimization process (solid line).

The parameter values obtained from the optimization processes (fitting the theoretical characteristics to experimental data) have been gathered and presented in Table 1.

It turned out that smaller current values observed for different points of the solar cell result mainly from different local serial and shunt resistances of this cell. The points exhibiting the minimum current are characterized by two times smaller shunt resistance and two times bigger serial resistance, with respect to the points exhibiting the maximum current.

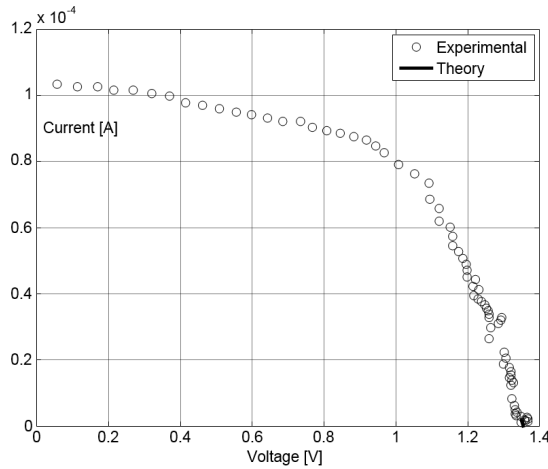


Fig. 10. The experimental data for the investigated silicon cell obtained at the minimum current point (circles) and the I–V theoretical curve calculated for parameter values obtained from the optimization process (solid line).

Table 1. The parameter values obtained for the investigated solar cell in two different points of the LBIC map.

	Max Current Point	Min Current Point
P_{max} [W]	$3.36 \cdot 10^{-4}$	$8.52 \cdot 10^{-5}$
I_{sc} [A]	$5.15 \cdot 10^{-4}$	$1.10 \cdot 10^{-4}$
V_{oc} [V]	1.23	1.35
FF [%]	0.53	0.57
R_{shunt} [Ω]	95900	47400
R_{serial} [Ω]	897.38	$1.69 \cdot 10^{-3}$

The next step was to investigate and analyze the U_{oc} voltage spectra of the solar cell. The experimental optical absorption coefficient spectra of amorphous and crystalline silicon types are presented in Fig. 11 below. The spectra have been measured with the same spectroscopic experimental set-up which has been described elsewhere [29, 30]. The amorphization level of silicon can be measured with the Photo-thermal Radiometry or Modulated Free Carrier Absorption methods described elsewhere [31, 32].

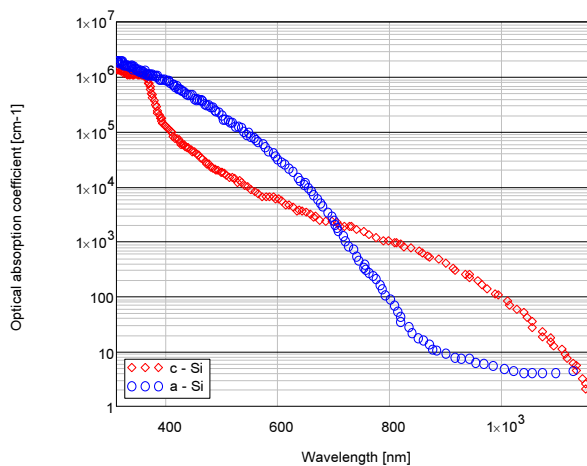


Fig. 11. The experimental optical absorption coefficient spectra of amorphous (circles) and crystalline (diamonds) silicon types.

The optical U_{oc} voltage spectra of the solar cell are presented in Fig. 12. In the first approximation the open circuit voltage U_{oc} spectrum depends on the optical absorption coefficient of the solar cell material and its active area thickness according to the proposed formulae (4–5):

$$U_{oc} = \frac{k_B T}{q} \ln \left[\frac{\eta I(\beta, d) \lambda q}{I_0 h c} \right], \quad (4)$$

$$I(\beta, d) = \int_0^d \beta(\lambda) \exp(-\beta(\lambda)x) dx, \quad (5)$$

where k_B is the Boltzmann constant, T is the temperature, q is the elementary charge, η is the quantum efficiency of photons to electrons, λ is the wavelength of illuminating light, I_0 is the reverse saturation current, h is the Planck constant, c is the speed of light, β is the optical absorption coefficient and d is the solar cell active region thickness.

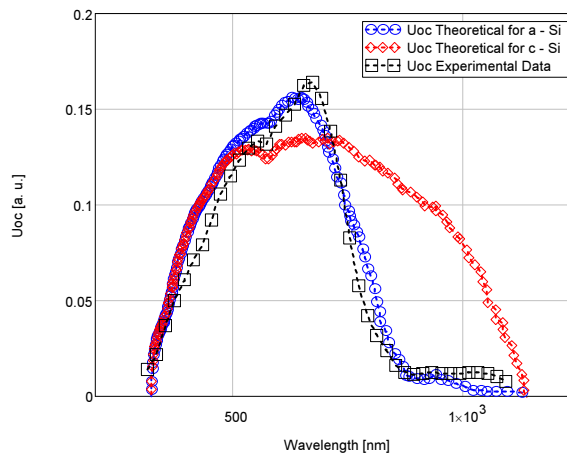


Fig. 12. The open circuit voltage experimental data obtained for the investigated solar cell (open boxes) and theoretical curves calculated for different optical absorption coefficient spectra (circles and diamonds).

The photo-voltage spectra for amorphous (circles) and crystalline (diamonds) silicon were computed for the optical absorption coefficient spectra presented in Fig. 11 and the solar cell active layer thickness $d = 1 \mu\text{m}$, typical for tandem type solar cells. Fig. 12 shows that fitting the computed and experimental characteristics is much better for the optical absorption spectrum of amorphous silicon than for crystalline silicon.

3. Conclusions

The Laser Beam Induced Current technique method offers several advantages compared to other techniques. It is a non-destructive method and allows for detection of defects which have a significant impact on solar cells energy and current efficiency. The analysis of photo-voltage spectra presented in the paper led us to the conclusion that it was the amorphous tandem type solar cell. The I–V characteristics have been measured in two different points and interpreted using a solar cell model based on the LambertW function. The essential parameters have been extracted for these points with the optimization methods. Smaller current efficiencies observed on the LBIC maps result from smaller shunt and bigger serial

resistances of the investigated solar cell, with respect to the points exhibiting bigger current efficiencies.

References

- [1] Quaschnig, V. (2004). Photovoltaic systems – Technology Fundamentals. *Manufacturing, Renewable Energy*, 1, 81–84.
- [2] Bell, R.O., Kalejs, J.P. (1998). Growth of silicon sheets for photovoltaic application. *Journal of Materials Research*, 13(10), 2732–2739.
- [3] Green, M.A. (2002). Photovoltaics Principles. *Physica E*, 14, 11–17.
- [4] Miles, R.W., Hynes, K.M., Forbes, I. (2005). Photovoltaic solar cells: An overview of state-of-the-art cell development and environmental issues. *Progress in Crystal Growth and Characterization of Materials*, 51, 1–42.
- [5] Guha, S., Yang, J., Banerjee, A., Glatfelter, T. (1998). Amorphous silicon alloy solar cells for space application. Vienna, Austria. *2nd World Conference & Exhibition on PV Solar Energy Conversion*, 3609–3612.
- [6] Osterwald, C.R. *Standards, calibration and testing of PV modules and solar cells*. (eds. Markvart, T., Castaner, L.). Practical Handbook of Photovoltaics, Elsevier, Kidlington Oxford, 793.
- [7] Emery, K. (2003). *Measurement and characterization of solar cells and modules*. (eds. Luque, A., Hegedus, S.). Handbook of Photovoltaic Science and Engineering, John Wiley & Sons Ltd, Chichester, UK, 701.
- [8] Würfel, P., Trupke, T., Puzzer, T., Schäffer, E., Warta, W., Glunz, S.W. (2007). Diffusion lengths of silicon solar cells from luminescence images. *Journal of Applied Physics*, 101, 123110.
- [9] Giesecke, J.A., Kasemann, M., Warta, W. (2009). Determination of local minority carrier diffusion lengths in crystalline silicon from luminescence images. *Journal of Applied Physics*, 106, 014907.
- [10] Kaminski, A., Jouglar, J., Mergui, M., Jourlin, Y., Bouillé, A., Vuillermoz, P.L., Laugier, A. (1998). Infrared characterization of hot spots in solar cells with high precision due to signal treatment processing. *Solar Energy Materials and Solar Cells*, 51, 233–242.
- [11] Hoppe, H., Bachmann, J., Muhsin, B., Drüe, K.H., Riedel, I., Gobsch, G., Buerhop-Lutz, C., Brabec, Ch.J., Dyakonov, V. (2010). Quality control of polymer solar modules by lock-in thermography. *Journal of Applied Physics*, 107, 014505.
- [12] Bachmann, J., Buerhop-Lutz, C., Deibel, C., Riedel, I., Hoppe, H., Brabec, C.J., Dyakonov, V. (2010). Organic solar cells characterized by dark lock-in thermography. *Solar Energy Materials and Solar Cells*, 94, 642–647.
- [13] Cole, E.I., (2004). Beam-Based Defect Localization Methods. *Microelectronics Failure Analysis (Materials Park: ASM International)*.
- [14] Zook, J.D., Maciolik, R.B., Heaps, J.D. (1980). Effects of Grain Boundaries in Polycrystalline Solar Cells. *Applied Physics Letters*, 37, 223–226.
- [15] Hari Rao, C.V., Bates, H.E., Ravi, K.V. (1976). Electrical Effects of SiC Inclusions in EFG Silicon Ribbon Solar Cells. *Journal of Applied Physics*, 47, 2614–2620.
- [16] Belouet, C., Hervo, J., Matres, R., Phuoc, N.T., Pertus, M. (1978). Growth and Characterization of Polysilicon Layers Achieved by the Ribbon-Against-Drop Process. *Proc. 13th IEEE Photovoltaics Specialists Conference*, 131–136.
- [17] Sawyer, W.D. (1986). An Improved Method of Light-Beam-Induced Current Characterization of Grain Boundaries. *Journal of Applied Physics*, 59, 2361–2368.
- [18] Galloway, S.A., Brinkman, A.W., Durose, K., Wilshaw, P.R., Holland, A.J., (1996). A Study of the Effects of Post-Deposition Treatment on CdS/CdTe Thin-Film Solar Cells Using High-Resolution optical beam induced current. *Applied Physics Letters*, 68, 3725–3727.

- [19] Li, G., Shrotriya, V., Huang, J., Yao, Y., Moriarty, T., Emery, K., Yang, Y. (2005). High-efficiency solution processable polymer photovoltaic cells by self-organization of polymer blends. *Nature Materials*, 4, 864–868.
- [20] Shirland, F. (1966). The history, design, fabrication and performance of CdS thin film solar cells. *Advanced Energy Conversion*, 6, 201–202.
- [21] Ouennoughi, Z., Chegaar, M. (1999). A simpler method for extracting solar cell parameters using the conductance method. *Solid-State Electronics*, 43, 1985–1988.
- [22] Nehaoua, N., Chergui, Y., Mekki, D.E. (2009). Determination of organic solar cell parameters based on single or multiple pin structures. *Vacuum*, 84, 326–329.
- [23] Chegaar, M., Azzouzi, G., Mialhe, P. (2006). Simple parameter extraction method for illuminated solar cells. *Solid-State Electronics*, 50, 1234–1237.
- [24] Bouzidi, K., Chegaar, M., Bouhemadou, A. (2007). Solar cells parameters evaluation considering the series and shunt resistance. *Solar Energy Materials and Solar Cells*, 91, 1647–1651.
- [25] Jain, A., Kapoor, A. (2005). A new method to determine the diode ideality factor of real solar cell using Lambert W-function. *Solar Energy Materials and Solar Cells*, 85, 391–396.
- [26] Jain, A., Kapoor, A. (2005). A new approach to study organic solar cell using Lambert function. *Solar Energy Materials and Solar Cells*, 86, 197–205.
- [27] Kunz, G., Wagner, A. (2004). Internal series resistance determined of only one IV-curve under illumination. *19th European Photovoltaic Solar Energy Conference, Paris, France*, Paper No. 5BV.2.70.
- [28] Zhang, Ch., Zhang, J., Hao, Y., Lin, Z., Zhu, Ch. (2011). A simple and efficient solar cell parameter extraction method from a single current-voltage curve. *Journal of Applied Physics*, 110, 064504.
- [29] Maliński, M., Chrobak, Ł. (2010). Photoacoustic operation modes for determination of absorption spectra of SiGe mixed crystals. *Opto-Electronics Review*, 18(2), 190–196.
- [30] Chrobak, Ł., Malinski, M., Strzalkowski, K., Zakrzewski, J. (2012). Energy efficiency of near infrared cobalt luminescence in ZnSe:Co determined by a photoacoustic method. *Opto-Electronics Review*, 20(1), 91–95.
- [31] Maliński, M., Pawlak, M., Chrobak, Ł., Pal, S., Ludwig, A. (2015). Monitoring of Amorfization of the Oxygen Implanted Layers in Silicon Wafers Using Photothermal Radiometry and Modulated Free Carrier Absorption. *Applied Physics A – Materials Science & Processing*, 118(3), 1009–1014.
- [32] Chrobak, Ł., Maliński, M., Pawlak, M. (2014). Measurements of the Optical Absorption Coefficient of Ar⁺⁸ Ion Implanted Silicon Layers Using the Photothermal Radiometry and the Modulated Free Carrier Absorption Methods. *Infrared Physics & Technology*, 67, 604–608.